separations

MDPI

Article

Ultrasound-Assisted Deep Eutectic Solvent Extraction of Total Flavonoids from Hainan Li-Medicine *Polygonum hydropiper*: Process Optimization, Antioxidant Activity and Molecular Mechanism

Xinyu Wang [1], Haoli Tian [1], Huayan Zhang [2] and Yahui Shan [1,*]

[1] School of Medicine, Hainan Vocational University of Science and Technology, Haikou 571137, China; wxy@hvust.edu.cn (X.W.); holly.tian@hvust.edu.cn (H.T.)
[2] Chuxiong Prefecture Inspection and Testing Certification Institute, Chuxiong 675000, China; 14769337248@163.com
* Correspondence: danyahui1@jxutcm.edu.cn; Tel.: +86-18070505523

Abstract

Ultrasound-assisted deep eutectic solvent (DES) extraction was developed for the efficient recovery of total flavonoids from *Polygonum hydropiper* L., a traditional Li medicinal plant from Hainan, China. Among 30 DES formulations screened, betaine-glycerol (Bet-Gly, 1:2) afforded the highest total flavonoid yield and was selected for further optimization. The extraction conditions were systematically optimized through single-factor experiments, Plackett–Burman screening, and Box–Behnken response-surface methodology. The predicted optimal conditions (water content 28.08%, solid-to-liquid ratio 1:37.58, and extraction time 30.69 min) were adjusted to 28.10%, 1:38, and 31 min for practical operation, yielding 3.98 mg RE/g DW, in close agreement with the predicted value of 4.13 mg RE/g DW. Compared with 70% ethanol and water, Bet-Gly increased the total flavonoid yield by 39.6% and 131.4%, respectively ($p < 0.05$), and the resulting extract showed the lowest IC_{50} values in both ABTS and DPPH radical-scavenging assays. UPLC-Q-TOF-MS/MS tentatively identified eight phenolic constituents, mainly flavonoids, in the DES extract. Molecular dynamics simulations further revealed more homogeneous distributions of five representative flavonoids and more favorable flavonoid-solvent interaction energies in Bet-Gly than in water or 70% ethanol, indicating that electrostatic and van der Waals interactions contributed to enhanced flavonoid solvation. Overall, this study integrates DES screening, process optimization, chemical characterization, antioxidant evaluation, and molecular simulation, linking the improved extraction performance of Bet-Gly with favorable flavonoid-solvent interactions at the molecular level.

Keywords: *Polygonum hydropiper* L.; deep eutectic solvents; ultrasound-assisted extraction; flavonoids; response surface methodology; antioxidant activity; UPLC-Q-TOF-MS/MS; molecular dynamics simulation

Check for updates

Academic Editor: Petr Bednar

Received: 17 September 2026
Revised: 8 October 2026
Accepted: 10 October 2026
Published: 15 October 2026

Copyright: © 2026 by the authors. Licensee MDPI, Basel, Switzerland. This article is an open access article distributed under the terms and conditions of the Creative Commons Attribution (CC BY) license.

1. Introduction

Polygonum hydropiper L. is an annual herb of the Polygonaceae family. It has a long history of use in the traditional medicine of the Li ethnic group of Hainan, China, mainly for dysentery, diarrhea, gastroenteritis, rheumatic pain, and pruritus [1]. The plant contains various bioactive constituents, including flavonoids, sesquiterpenes, and volatile oils, of which

flavonoids are closely associated with its antioxidant, anti-inflammatory, and antibacterial activities [2]. Peng et al. isolated 10 flavonoids from the leaves of *P. hydropiper* and reported their pronounced antioxidant activity [3]. However, the green and efficient extraction and systematic utilization of these flavonoids have received little attention. An efficient and environmentally friendly extraction strategy is therefore needed to support the further utilization of the bioactive constituents of *P. hydropiper*.

Conventional organic solvents, such as ethanol and methanol, are still widely used for the extraction of flavonoids from *P. hydropiper*. However, their extensive use is associated with solvent consumption, volatility, and potential environmental and residue concerns, which are not fully consistent with the principles of green and sustainable extraction [4]. Deep eutectic solvents (DESs) are generally formed by combining hydrogen bond acceptors (HBAs) and hydrogen bond donors (HBDs) through intermolecular interactions and have attracted considerable attention since the pioneering work of Abbott et al. on choline chloride–urea mixtures [5]. When DESs are composed of naturally occurring constituents, such as organic acids, sugars, amino acids, polyols, and choline derivatives, they are commonly referred to as natural deep eutectic solvents (NADESs) [6]. Compared with conventional organic solvents, DESs, particularly NADESs, generally exhibit low volatility, high tunability, and potentially favorable biocompatibility and biodegradability, while providing good solubilization and extraction capacities for a wide range of flavonoids [7,8]. These properties make DESs promising solvent systems for the green and efficient extraction of flavonoids from *P. hydropiper*.

Ultrasound-assisted extraction (UAE) is an efficient technique that enhances mass transfer and shortens extraction time mainly through acoustic cavitation and the associated mechanical effects [9]. In recent years, UAE combined with DESs has been increasingly applied to extract flavonoids and phenolic compounds from various plant materials, including the leaves of *Cercis glabra* [10], *Perilla frutescens* [11], *Moringa oleifera* [12], and Chinese bayberry [13], yielding favorable extraction efficiency and selectivity [14]. Among these systems, betaine-based DESs have received increasing interest for the green extraction of polyphenols and flavonoids. This interest reflects their tunable solvent properties and their ability to establish diverse intermolecular interactions with target compounds [15]. However, systematic studies on ultrasound-assisted DES extraction of flavonoids from *P. hydropiper* remain scarce, particularly those that screen and optimize betaine-based systems and probe their extraction mechanisms.

Flavonoids are widely recognized for their antioxidant properties, which are commonly associated with free-radical scavenging and the attenuation of oxidative damage. Accordingly, ABTS and DPPH radical-scavenging assays are widely used to evaluate the in vitro antioxidant capacity of natural products [16]. Previous studies have shown that the choice of extraction solvent affects not only flavonoid yield and composition but also the antioxidant performance of the resulting extracts. Extracts obtained with some DES systems have shown enhanced radical-scavenging activity [17]. However, the molecular mechanisms underlying DES-enhanced flavonoid extraction have not yet been fully elucidated. Molecular dynamics (MD) simulations and density functional theory (DFT) studies suggest that flavonoid solvation in DESs is governed jointly by hydrogen-bonding interactions, solute–solvent interactions, molecular aggregation, and solvent polarity [18]. Intermolecular interaction energies can provide further insight into the affinity between the solvent and the target compounds [19,20]. Nevertheless, direct evidence for the molecular interactions and solvation behavior of the major *P. hydropiper* flavonoids in specific DES systems is still lacking.

The present study aimed to develop a green and efficient strategy for extracting total flavonoids from *P. hydropiper* and to investigate the molecular basis underlying DES-

enhanced flavonoid extraction. First, 30 DESs with different HBA/HBD combinations were prepared and screened on the basis of total flavonoid yield. The extraction conditions were then optimized by single-factor experiments, a Plackett–Burman design, and Box–Behnken response-surface methodology. The optimized DES system was compared with 70% ethanol and water in terms of total flavonoid yield and ABTS and DPPH radical-scavenging activities. The chemical composition of the DES extract was subsequently qualitatively characterized by UPLC-Q-TOF-MS/MS. Finally, hyperoside, epicatechin, kaempferol, quercetin, and kaempferol-3-O-hexoside were selected as representative flavonoids for MD simulations, which compared their intermolecular interactions and solvation behavior in the DES, water, and 70% ethanol systems. Collectively, these analyses provide molecular-level insight into the enhanced extraction of flavonoids from *P. hydropiper* by DESs.

2. Materials and Methods

2.1. Materials and Reagents

A TripleTOF 5600 high-resolution mass spectrometer (SCIEX, Framingham, MA, USA) was used for analysis. *P. hydropiper* samples were collected from cultivated plants in Wenchang, Hainan Province, China, and authenticated by Professor Yinkui De of Hainan Vocational University of Science and Technology. The aerial parts were collected, dried, ground into powder, and passed through a 40-mesh sieve before use. Rutin reference standard (purity $\geq$ 98%) was purchased from Shanghai yuanye Bio-Technology Co., Ltd., Shanghai, China Ethanol, betaine, choline chloride, L-proline, glycerol, propylene glycol, urea, lactic acid, and other reagents were purchased from Shanghai Aladdin Biochemical Technology Co., Ltd., Shanghai, China ABTS, DPPH, potassium persulfate, L-ascorbic acid (VC), acetonitrile, and formic acid were obtained from FTSCI (Hubei) Science and Technology Co., Ltd., Wuhan, China Ultrapure water was used throughout the experiments, and all other reagents were of analytical grade.

2.2. Preparation of DES Systems

DESs were prepared according to previously reported methods with minor modifications [21,22]. The HBA/HBD combinations and molar ratios were selected based on previously reported DES formulations. Because different HBA/HBD combinations possess distinct molecular structures and hydrogen-bonding capacities, different molar ratios were selected for different DES systems [23,24]. Accordingly, literature-supported molar ratios ranging from 1:1 to 1:4 were adopted for the initial DES screening. The HBA and HBD were mixed at the molar ratios shown in Table 1 and stirred at 80 °C and 350 rpm until a homogeneous liquid was formed.

Table 1. Preparation of DESs with different components and total flavonoid yields from *P. hydropiper*.

No.	HBAs	HBDs	Molar Ratio	Yield (mg RE/g DW)
DES-1	ChCl	Propylene glycol	1:4	2.48 ± 0.38
DES-2		Glycerol	1:2	1.15 ± 0.35
DES-3		Urea	1:1	2.28 ± 0.43
DES-4		Lactic acid	1:2	2.21 ± 0.18
DES-5		DL-Malic acid	1:1	2.15 ± 0.45
DES-6		Citric acid	1:1	2.86 ± 0.15
DES-7		Glucose	1:1	2.93 ± 0.45
DES-8		Fructose	1:1	1.26 ± 0.40
DES-9		Sorbitol	1:2	0.71 ± 0.32
DES-10		Xylitol	1:1	1.03 ± 0.30
DES-11	BET	Propylene glycol	1:4	3.14 ± 0.45
DES-12		Glycerol	1:2	3.29 ± 0.43
DES-13		Urea	1:1	3.23 ± 0.37

Table 1. *Cont.*

No.	HBAs	HBDs	Molar Ratio	Yield (mg RE/g DW)
DES-14	BET	Lactic acid	1:2	2.75 ± 0.40
DES-15		DL-Malic acid	1:1	2.62 ± 0.33
DES-16		Citric acid	1:1	1.70 ± 0.50
DES-17		Glucose	1:1	2.02 ± 0.33
DES-18		Fructose	1:1	1.95 ± 0.45
DES-19		Sorbitol	1:2	2.33 ± 0.43
DES-20		Xylitol	1:1	3.26 ± 0.41
DES-21	Pro	Propylene glycol	1:4	2.90 ± 0.38
DES-22		Glycerol	1:2	1.96 ± 0.44
DES-23		Urea	1:1	1.90 ± 0.34
DES-24		Lactic acid	1:2	2.18 ± 0.43
DES-25		DL-Malic acid	1:1	2.37 ± 0.33
DES-26		Citric acid	1:1	2.13 ± 0.42
DES-27		Glucose	1:1	2.93 ± 0.43
DES-28		Fructose	1:1	1.86 ± 0.37
DES-29		Sorbitol	1:2	1.70 ± 0.32
DES-30		Xylitol	1:1	2.31 ± 0.43

2.3. Determination of Total Flavonoid Yield

2.3.1. Construction of the Calibration Curve

Different volumes (0, 0.6, 1.0, 1.2, 1.4, 1.6, 1.8, and 2.0 mL) of a rutin standard solution (0.512 mg/mL) were transferred into 20 mL volumetric flasks. Next, 1 mL of 5% $NaNO_2$ solution, 1 mL of 10% $Al(NO_3)_3$ solution, and 4 mL of 1 mol/L NaOH solution were added sequentially. The solutions were diluted to volume with 50% ethanol, mixed thoroughly, and allowed to stand for 10 min. Using 50% ethanol as the blank, the absorbance was measured at 510 nm. A calibration curve was constructed by plotting rutin concentration (x, μg/mL) against absorbance (A).

2.3.2. Calculation of Total Flavonoid Yield

The total flavonoid concentration was calculated using the linear regression equation of the rutin calibration curve. The total flavonoid yield was then calculated with Equation (1).

$$Y = C \times V \times D/m \quad (1)$$

where Y is the total flavonoid yield (mg RE/g DW), C is the flavonoid concentration from the calibration curve (mg/mL), V is the extraction volume (mL), D is the dilution factor, and m is the sample mass (g).

2.4. Screening of DESs for Flavonoid Extraction

Thirty 1.0 g portions of powdered *P. hydropiper* were accurately weighed. Each sample was extracted with 20 mL of one of the 30 prepared DES systems (water content of 40%) at 50 °C [25] using UAE at 85 W for 30 min. After extraction, the extracts were centrifuged at 5000 rpm for 15 min, and the supernatants were collected and stored under refrigeration until analysis. The total flavonoid yield was determined as described in Section 2.3. The DES system with the highest total flavonoid yield was selected as the optimal extraction solvent.

2.5. Optimization of DES-Based Extraction Conditions

2.5.1. Single-Factor Experiments

After the optimal DES system was identified, single-factor experiments were performed to investigate the effects of different extraction parameters on the total flavonoid yield. The effects of water content (10%, 20%, 30%, 40%, and 50%), solid-to-liquid ratio

(1:10, 1:20, 1:30, 1:40, and 1:50), extraction time (10, 20, 30, 40, and 50 min), ultrasonic power (80, 90, and 100 W), and extraction temperature (40, 50, 60, 70, and 80 °C) were evaluated. The key factors and their levels for subsequent response-surface optimization were determined from the single-factor results.

2.5.2. Plackett–Burman Design (PBD)

Based on the single-factor experiments, a Plackett–Burman design was applied to identify the critical factors affecting total flavonoid yield. Five variables, water content (X_1), solid-to-liquid ratio (X_2), extraction time (X_3), ultrasonic power (X_4), and extraction temperature (X_5), were investigated at two levels in a 12-run design. The total flavonoid yield was used as the response variable. The regression model was analyzed with Design-Expert 13.0 software to determine the significant factors influencing extraction [26].

2.5.3. Box–Behnken Response Surface Optimization

Based on the single-factor experiments and the Plackett–Burman design, three significant factors, water content (X_1), solid-to-liquid ratio (X_2), and extraction time (X_3), were selected for further optimization. A three-factor, three-level Box–Behnken design (BBD) was constructed using Design-Expert 13.0 software. A quadratic regression model was established, and analysis of variance (ANOVA) was performed to evaluate the model significance. The optimal extraction conditions were determined, and three independent validation experiments were conducted to verify the reliability of the model.

2.6. Comparison of Extraction Performance Among Different Solvent Systems

Under the optimized conditions, the optimal DES, water, and 70% ethanol were used to extract flavonoids from *P. hydropiper*. The total flavonoid yield was determined as described in Section 2.3. All experiments were performed in triplicate, and the extraction performance of the different solvent systems was compared.

2.7. In Vitro Antioxidant Activity Assays

2.7.1. ABTS Radical-Scavenging Assay

The ABTS radical-scavenging activity was determined according to the method described by Guo [27] with slight modifications. The ABTS stock solution was prepared by mixing equal volumes of 7 mmol/L ABTS solution and 2.4 mmol/L potassium persulfate solution, followed by incubation in the dark at low temperature for 12 h. Before use, the stock solution was diluted with phosphate-buffered saline (PBS) to an absorbance of 0.70 ± 0.02 at 734 nm to obtain the ABTS working solution. For the positive control, a 200 μg/mL VC stock solution was prepared and subsequently diluted to concentrations of 2, 4, 10, 20, 25, 40, 50, and 100 μg/mL. Meanwhile, the *P. hydropiper* extracts were diluted with PBS to obtain sample solutions at concentrations of 0.173, 0.186, 0.217, 0.260, 0.325, 0.433, 0.650, and 0.867 mg/mL for subsequent analysis.

For determination of the radical-scavenging activity, 2 mL of the diluted ABTS working solution was mixed with 100 μL of PBS as the control (A_0), whereas 2 mL of the ABTS working solution was mixed with 100 μL of sample solution as the sample (A_i). The mixtures were incubated in the dark at room temperature for 8 min, after which the absorbance was measured at 734 nm. All measurements were performed in triplicate, and VC was used as the positive control. The ABTS radical-scavenging rate was calculated according to Equation (2), and the IC_{50} values of the *P. hydropiper* extracts were subsequently determined.

$$\text{ABTS radical-scavenging rate} = \frac{A_0 - A_i}{A_0} \times 100\% \quad (2)$$

where A_0 is the absorbance of the control mixture containing 2 mL of ABTS working solution and 100 µL of PBS, and A_i is the absorbance of the mixture containing 2 mL of ABTS working solution and 100 µL of sample solution.

2.7.2. DPPH Radical-Scavenging Assay

The DPPH radical-scavenging activity was determined according to a previously reported method with slight modifications [28]. A 0.2 mmol/L DPPH solution was prepared for subsequent analysis. VC was used as the positive control. A VC stock solution at a concentration of 0.200 mg/mL was prepared and further diluted to concentrations of 0.005, 0.010, 0.020, 0.025, 0.040, 0.050, 0.100, and 0.200 mg/mL. Meanwhile, the *P. hydropiper* extracts were diluted with ethanol to obtain sample solutions at concentrations of 0.650, 0.867, 1.300, 2.800, 3.250, 4.333, 6.500, and 13.000 mg/mL. Based on preliminary range-finding experiments, the concentration ranges for the ABTS and DPPH assays were selected separately to obtain appropriate concentration–response curves for reliable IC_{50} determination. A broader and higher concentration range was therefore employed in the DPPH assay because higher extract concentrations were required to achieve measurable radical-scavenging responses under the present experimental conditions. For determination of the DPPH radical-scavenging activity, 2 mL of DPPH solution was mixed with 100 µL of absolute ethanol to obtain the blank control (A_0). A sample reaction mixture was prepared by mixing 2 mL of DPPH solution with 100 µL of sample solution (A_1). In addition, 2 mL of absolute ethanol was mixed with 100 µL of sample solution to obtain the sample background (A_2). All mixtures were incubated in the dark at room temperature for 30 min, and the absorbance was measured at 517 nm. All experiments were performed in triplicate. The DPPH radical-scavenging rate was calculated according to Equation (3), and the IC_{50} values of the different *P. hydropiper* extracts were subsequently determined from their DPPH radical-scavenging rates.

$$\text{DPPH radical-scavenging rate} = [1 - (A_1 - A_2)/A_0] \times 100\% \quad (3)$$

where A_0 is the absorbance of the blank control, A_1 is the absorbance of the sample reaction mixture, and A_2 is the absorbance of the sample background.

2.8. UPLC-Q-TOF-MS/MS Analysis

Chromatographic separation was performed on an ACQUITY UPLC BEH C18 column (2.1 × 100 mm, 1.7 µm). The mobile phase consisted of 0.1% aqueous formic acid (A) and acetonitrile (B) with the following gradient: 0–1 min, 5% B; 1–5 min, 5–35% B; 5–30 min, 35–95% B; 30–33 min, 95% B; 33–33.1 min, 95–5% B; 33.1–35 min, 5% B. The column temperature was maintained at 40 °C, the injection volume was 1 µL, and the flow rate was 0.3 mL/min. Mass spectrometric analysis was performed using an electrospray ionization (ESI) source in both positive and negative ion modes. The ion spray voltage (ISVF) was set at 5.5 kV and −4.5 kV for positive and negative ion modes, respectively. The declustering potential (DP) was ±100 V, and the collision energy (CE) was ±38 V. The mass scan range was m/z 100–1500, the ion source temperature (TEM) was maintained at 500 °C, and the collision energy spread (CES) was set to 15 V. The curtain gas pressure (CUR) was 40 psi, and the nebulizer gas pressure (GS1) and auxiliary gas pressure (GS2) were both set at 50 psi. Data acquisition was performed for 35 min.

2.9. Molecular Dynamics Simulation

We used molecular dynamics (MD) simulation to investigate the interaction mechanism between flavonoid compounds and different extraction solvent systems, using the GROMACS 2023.3 software package. The GAFF force field was employed. The topology

files for five flavonoids (hyperoside, epicatechin, kaempferol, quercetin, and kaempferol-3-*O*-hexoside) were generated with Sobtop [29]. Geometry optimization and restrained electrostatic potential (RESP) charge calculations were performed at the B97-3c level for all structures using ORCA (Version 5.0) [30] and Multiwfn (Version 3.8) [31]. Three simulation systems, water, Bet-Gly, and 70% EtOH, were constructed. Each system contained 10 molecules of each of the five representative flavonoids (hyperoside, epicatechin, kaempferol, quercetin, and kaempferol-3-O-hexoside), corresponding to a total of 50 flavonoid molecules. The water system contained 16,891 water molecules. The Bet-Gly system contained 900 betaine molecules, 1800 glycerol molecules, and 5883 water molecules, maintaining a betaine:glycerol molar ratio of 1:2 and a water content of 28.10% (w/w). The 70% EtOH system contained 3669 ethanol molecules and 5085 water molecules, corresponding approximately to 70% ethanol (v/v). The initial configurations were generated in a cubic box of $8 \times 8 \times 8$ nm^3 using Packmol (Version 20.14.4) [32]. The initial structures were energy-minimized by the steepest descent algorithm followed by conjugate-gradient optimization, with a convergence criterion of a maximum force below 10 kJ/(mol·nm). The systems were then heated to 343.15 K over 100 ps in the NVT ensemble under periodic boundary conditions with a 2 fs time step. All covalent bonds involving hydrogen atoms were constrained with the LINCS algorithm [33], and the temperature was coupled to the V-rescale thermostat. Electrostatic interactions were treated with the particle-mesh Ewald (PME) method [34] using a 1.4 nm real-space cutoff, and the same cutoff was used for van der Waals interactions. After heating, the systems were equilibrated for 100 ps in the NPT ensemble under identical constraints and time steps, with the pressure maintained at 1.0 atm by the Parrinello–Rahman barostat [35,36]. Production simulations were then run for 100 ns per system under equilibrium conditions (343.15 K, 1 atm) with a 2 fs time step. MD trajectories were analyzed with GROMACS utilities, including gmx hbond for hydrogen-bonding patterns, gmx gyrate for the radius of gyration, and gmx rms for the root-mean-square deviation (RMSD). Structural visualization and trajectory analysis were performed with VMD 1.9.3 [37] and PyMOL 3.0 [38].

2.10. Statistical Analysis

All assays were carried out in triplicate, and the results are expressed as mean ± standard deviation (SD).

3. Results and Discussion

3.1. Construction of the Calibration Curve for Total Flavonoid Yield Determination

A calibration curve was established using rutin as the reference standard for the determination of total flavonoid yield. As shown in Figure A1, a good linear relationship was observed between rutin concentration and absorbance over the range of 15.36–51.20 μg/mL. The regression equation was:

$$A = 0.01337x - 7.21491 \times 10^{-4}, R^2 = 0.99959.$$

3.2. Evaluation of DESs for Flavonoid Extraction

To evaluate the extraction performance of different DES systems, 30 DESs prepared with various hydrogen bond acceptors (HBAs) and hydrogen bond donors (HBDs) were used to extract flavonoids from *P. hydropiper*. As shown in Table 1, total flavonoid yield differed markedly among the tested DES systems, indicating that DES composition strongly influenced extraction efficiency. Among the investigated DESs, the betaine–glycerol system (Bet-Gly) at a molar ratio of 1:2 gave the highest total flavonoid yield (3.29 mg RE/g DW), reflecting its superior extraction capability for the flavonoids of *P. hydropiper*. By comparison,

DESs based on choline chloride as the HBA, or those containing other HBDs, gave relatively lower yields. These differences in extraction performance may be attributed to variations in polarity, viscosity, hydrogen-bonding interactions, and solvation capacity arising from different HBA/HBD combinations [39]. Bet-Gly (1:2) was therefore selected as the optimal DES for subsequent ultrasound-assisted extraction optimization.

3.3. Effect of Single Factors on Total Flavonoid Yield

3.3.1. Effect of Water Content

The effect of water content on total flavonoid yield was investigated, and the results are shown in Figure 1A. As water content increased, total flavonoid yield rose gradually and reached a maximum at 30%. A further increase in water content (40–50%) led to a decline in yield. An appropriate amount of water reduces DES viscosity and improves solvent penetration and mass transfer, thereby facilitating the dissolution of flavonoids [40]. Excessive water, however, may disrupt the hydrogen-bonding network of the DES and weaken solvent–solvent interactions, reducing extraction efficiency [41]. A water content of 30% was therefore selected as the optimal level for subsequent experiments.

3.3.2. Effect of Solid-to-Liquid Ratio

The influence of the solid-to-liquid ratio on total flavonoid yield is presented in Figure 1B. When the ratio increased from 1:10 to 1:20, only slight changes in total flavonoid yield were observed. With a further increase in solvent volume, total flavonoid yield increased rapidly and reached a maximum at a ratio of 1:40. A larger solvent volume provides sufficient contact between DES molecules and plant material, promoting the diffusion and dissolution of flavonoids. However, an excess of solvent may not further improve extraction efficiency and increases solvent consumption [42]. A solid-to-liquid ratio of 1:40 was therefore selected for subsequent optimization.

3.3.3. Effect of Extraction Time

The effect of extraction time on total flavonoid yield is shown in Figure 1C. Total flavonoid yield increased gradually with prolonged extraction time and reached a maximum at 30 min. A further extension to 50 min, however, resulted in a marked decrease in yield. The variation in yield with extraction time may be attributed to the combined effects of ultrasonic cavitation and flavonoid stability [43]. Insufficient extraction time may limit the dissolution and diffusion of flavonoids from the plant matrix, whereas prolonged ultrasonic treatment may generate localized heating and reactive species that compromise the structural stability of the DES and promote flavonoid degradation or oxidation, ultimately reducing yield [44]. An extraction time of 30 min was therefore selected as optimal.

3.3.4. Effect of Ultrasonic Power

The effect of ultrasonic power on total flavonoid yield is shown in Figure 1D. Total flavonoid yield increased with increasing ultrasonic power within the investigated range. This may be attributed to the enhanced cavitation generated at higher ultrasonic intensity, which facilitates the disruption of plant cell structures and improves contact between the solvent and intracellular components, thereby promoting flavonoid release [45]. An ultrasonic power of 100 W was therefore selected for subsequent experiments.

3.3.5. Effect of Extraction Temperature

The influence of extraction temperature on total flavonoid yield is presented in Figure 1E. Total flavonoid yield increased gradually with increasing temperature and reached a maximum at 70 °C. This increase may be related to the reduction in DES viscosity and the enhancement of molecular diffusion at elevated temperatures, which facilitates solvent

penetration and flavonoid dissolution [46]. A further increase in temperature, however, reduced total flavonoid yield, possibly because excessive temperature adversely affects flavonoid stability and promotes degradation reactions [43]. A temperature of 70 °C was therefore selected as optimal for subsequent experiments.

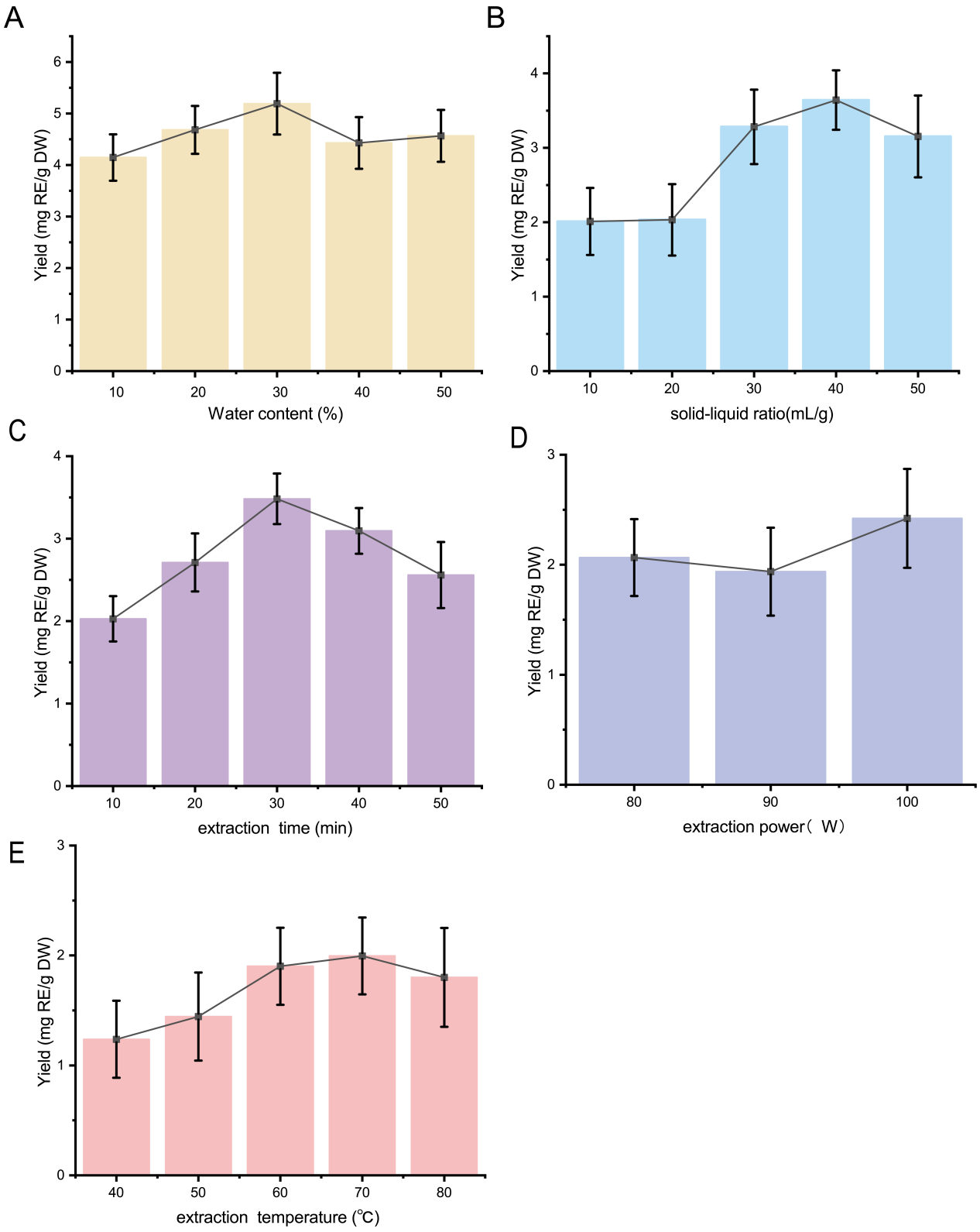


Figure 1. Effects of single factors on total flavonoid yield from *Polygonum hydropiper*. (**A**) Effect of water content; (**B**) Effect of solid-to-liquid ratio; (**C**) Effect of extraction time; (**D**) Effect of extraction power; (**E**) Effect of extraction temperature.

3.4. Identification of Key Factors by Plackett–Burman Design (PBD) Screening

PBD was employed to identify the significant factors affecting total flavonoid yield using a limited number of runs. Based on the single-factor results, five variables, water content (X1), solid-to-liquid ratio (X2), extraction time (X3), ultrasonic power (X4), and extraction temperature (X5), were selected for PBD analysis. The data in Table A1 were subjected to regression analysis, and the regression equation for total flavonoid yield was obtained as follows:

$Y = +3.68 + 0.6835X_1 - 0.3278X_2 + 0.3332X_3 + 0.1555X_4 + 0.1835X_5$. ANOVA results are presented in Table 2. The model was significant ($p < 0.01$), indicating that the regression model was reliable for identifying the key factors affecting total flavonoid yield. As shown in the Pareto chart (Figure 2), variables exceeding the *t*-value reference line were considered to have significant effects on the response. In the half-normal probability plot, variables showing greater deviation from the reference line were considered to contribute more significantly to the response [47]. The factors that significantly affected total flavonoid yield were X_1 (water content), X_2 (solid-to-liquid ratio), and X_3 (extraction time). PBD therefore identified X_1, X_2, and X_3 as the key variables for subsequent optimization.

Table 2. ANOVA for the Plackett–Burman model of total flavonoid yield.

Source	Sum of Squares	df	Mean Square	F-Value	*p*-Value	
Model	8.92	5	1.78	24.06	0.0007	significant
A-X_1	5.61	1	5.61	75.59	0.0001	
B-X_2	1.29	1	1.29	17.39	0.0059	
C-X_3	1.33	1	1.33	17.96	0.0055	
D-X_4	0.2902	1	0.2902	3.91	0.0953	
E-X_5	0.4041	1	0.4041	5.45	0.0583	
Residual	0.4450	6	0.0742			
Cor Total	9.37	11				

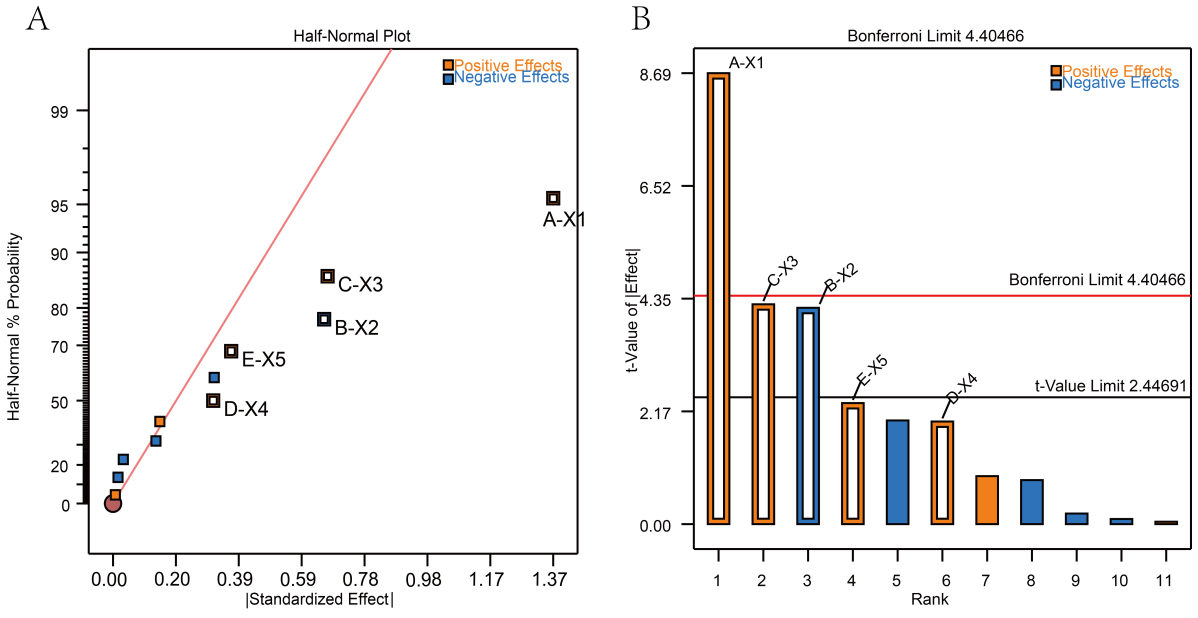


Figure 2. Pareto chart and half-normal plot showing the effects of five variables on total flavonoid yield: X_1 (water content), X_2 (solid-to-liquid ratio), X_3 (extraction time), X_4 (ultrasonic power), and X_5 (extraction temperature). (**A**) Half-normal plot of the standardized effects. The red line represents the reference line. Orange and blue squares indicate positive and negative effects, respectively. (**B**) Pareto chart showing the standardized effects ranked by their absolute values. The orange and blue bars represent positive and negative effects, respectively. The red and black horizontal lines represent the Bonferroni limit and the *t*-value limit, respectively.

3.5. Analysis of Box–Behnken Response Surface Optimization

Based on the single-factor results and the PBD, three significant factors, water content (X_1), solid-to-liquid ratio (X_2), and extraction time (X_3), were selected for further optimization. A three-factor, three-level Box–Behnken design (BBD) was performed, and 17 experimental runs (Table A2) were conducted using Design-Expert 13.0 software. The experimental data were fitted with a quadratic regression model, and the relationship between the independent variables and total flavonoid yield was described by the following equation:

$$Y = 4.05 - 0.2511X_1 - 0.4105X_2 + 0.1478X_3 + 0.2169X_1X_2 + 0.3559X_1X_3 - 0.2699X_2X_3 - 0.7272X_1^2 - 0.9728X_2^2 - 1.05X_3^2$$

ANOVA results (Table 3) demonstrated that the quadratic model was highly significant ($p < 0.0001$), whereas the lack-of-fit test was not significant ($p = 0.8694$), indicating good agreement between the model and the experimental data. The coefficient of determination (R^2) was 0.9914, and the coefficient of variation (CV) was 4.95%, suggesting satisfactory reliability and reproducibility of the model. Based on the regression coefficients, the effects of the three variables on total flavonoid yield followed the order $X_2 > X_1 > X_3$, indicating that the solid-to-liquid ratio had the greatest influence on extraction efficiency.

Table 3. ANOVA for the Box–Behnken quadratic model of total flavonoid yield.

Source	Sum of Squares	df	Mean Square	F-Value	*p*-Value	
Model	15.08	9	1.68	89.75	<0.0001	significant
A-X_1	0.5043	1	0.5043	27.02	0.0013	
B-X_2	1.35	1	1.35	72.22	<0.0001	
C-X_3	0.1747	1	0.1747	9.36	0.0183	
AB	0.1882	1	0.1882	10.08	0.0156	
AC	0.5066	1	0.5066	27.14	0.0012	
BC	0.2914	1	0.2914	15.61	0.0055	
A^2	2.23	1	2.23	119.28	<0.0001	
B^2	3.98	1	3.98	213.47	<0.0001	
C^2	4.62	1	4.62	247.42	<0.0001	
Residual	0.1307	7	0.0187			
Lack of Fit	0.0194	3	0.0065	0.2330	0.8694	not significant
Pure Error	0.1112	4	0.0278			
Cor Total	15.21	16				
R^2		0.9914				
Adjusted R^2		0.9804				
Predicted R^2		0.9681				
C.V. %		4.95				
AP		24.3619				

The response surface and contour plots (Figure 3) illustrated the interactions among the three variables and their effects on total flavonoid yield. The elliptical contour plots revealed interactions among the variables, with the interaction between water content and extraction time exerting a stronger influence than the other combinations. The maximum response region was located near the center of the experimental design space, indicating that moderate levels of the three variables were favorable for flavonoid extraction.

3.6. Comparison of Extraction Efficiency of Different Solvents

Under the optimized extraction conditions, the extraction efficiencies of Bet-Gly, 70% ethanol, and water were compared. The total flavonoid yields obtained with Bet-Gly, 70% ethanol, and water were 3.98, 2.85, and 1.72 mg RE/g DW, respectively. Compared with 70% ethanol and water, Bet-Gly increased total flavonoid yield by 39.6% and 131.4%, respectively, and these differences were statistically significant ($p < 0.05$).

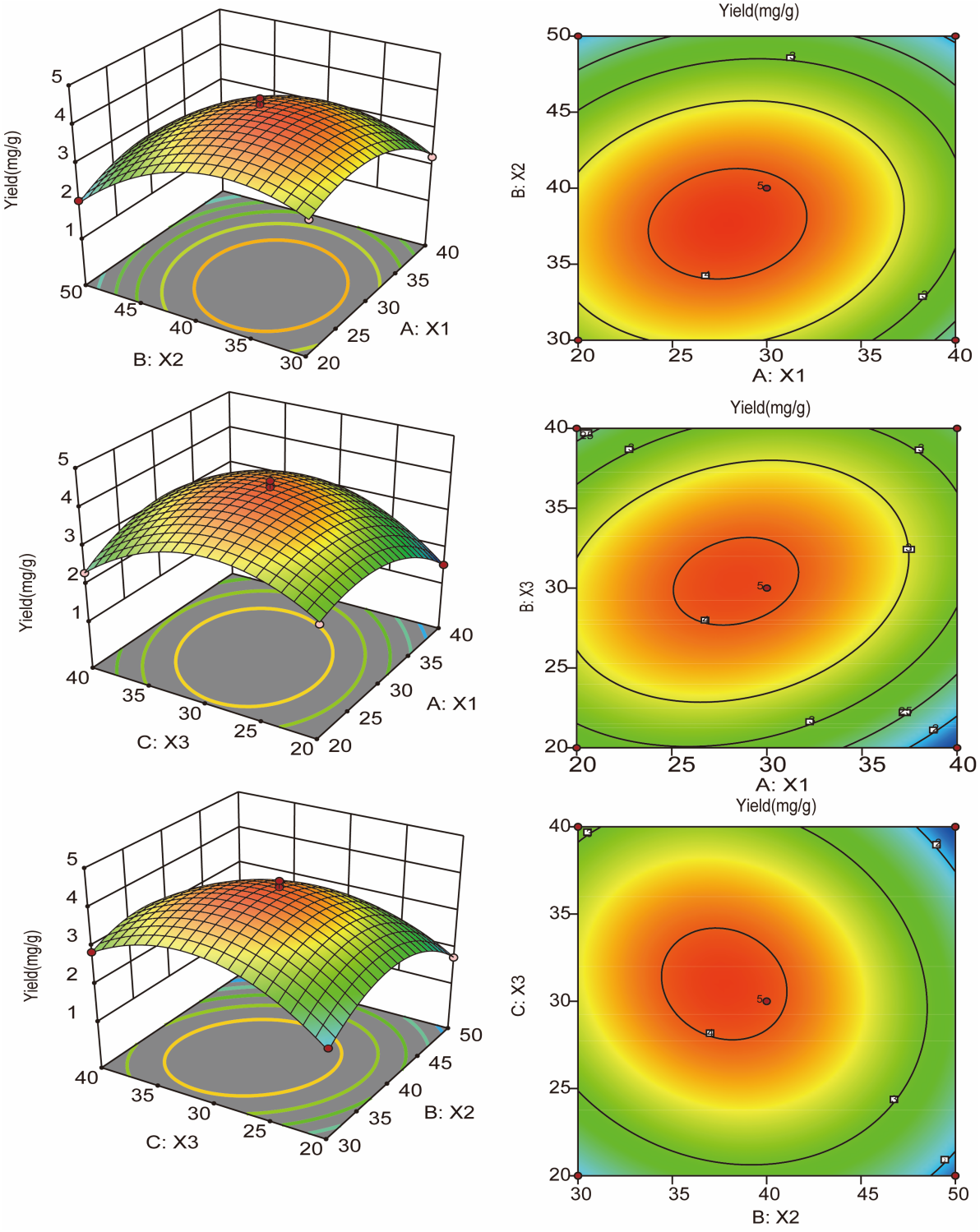


Figure 3. Contour and response surface plots showing the interactions of the three variables (A: X_1 water content; B: X_2 solid-to-liquid ratio; C: X_3 extraction time).

3.7. In Vitro Antioxidant Activity

The in vitro antioxidant activities of the three extracts were evaluated using ABTS and DPPH radical-scavenging assays, and the results are shown in Figure 4. The radical-scavenging rates of all extracts rose in a concentration-dependent manner, indicating that antioxidant capacity increased with extract concentration. Compared with the 70% ethanol and water extracts, the DES extract exhibited significantly stronger ABTS and DPPH radical-scavenging activity ($p < 0.05$). The DES extract also showed the lowest IC_{50} values (see

Table A3) in both assays, followed by the 70% ethanol and water extracts, demonstrating its superior antioxidant capacity. The enhanced antioxidant activity of the DES extract may be associated with its more efficient extraction of flavonoids, which are important contributors to antioxidant activity [48]. Similar improvements in antioxidant activity have been reported for flavonoid extracts obtained with DES-based extraction systems [49].

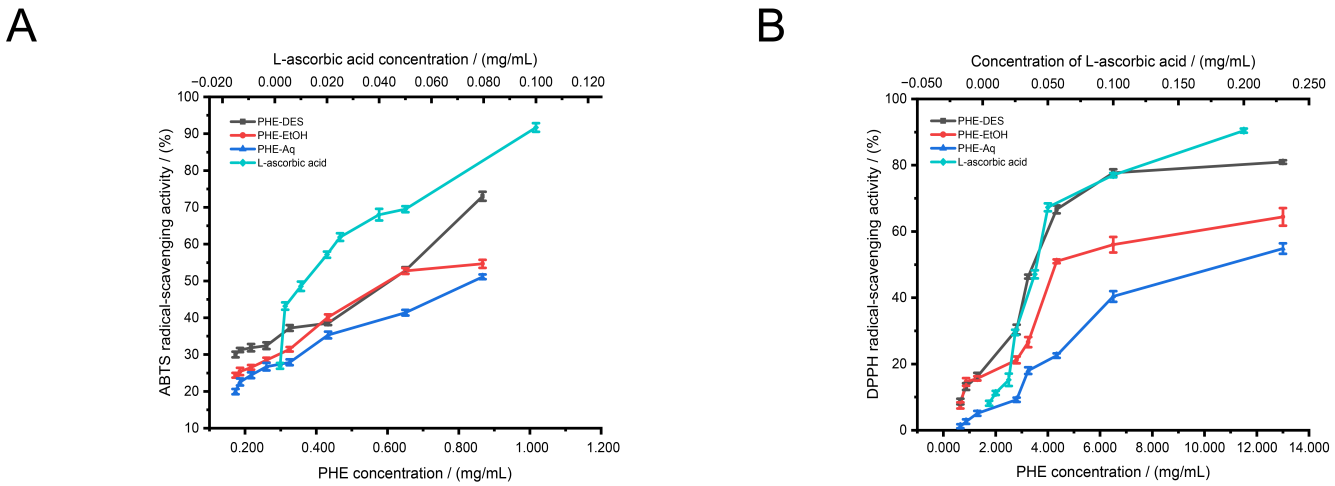


Figure 4. Antioxidant capacity of *Polygonum hydropiper* extracts obtained with different solvents. (**A**) ABTS radical-scavenging assay; (**B**) DPPH radical-scavenging assay. PHE-DES, PHE-EtOH, and PHE-Aq correspond to the DES, 70% ethanol, and water extracts, respectively. L-ascorbic acid served as the positive control.

3.8. Identification of Chemical Constituents by UPLC-Q-TOF-MS/MS

The flavonoid constituents in the DES extract of *P. hydropiper* were rapidly analyzed and tentatively identified by UPLC-Q-TOF-MS/MS. The total ion chromatogram (TIC) of the DES extract is shown in Figure 5. A total of eight flavonoids and related phenolic compounds were tentatively identified based on their accurate masses, retention times, and characteristic MS/MS fragmentation patterns. The identified compounds are summarized in Table 4. Compound **1** exhibited a retention time of 1.43 min. In the negative ion mode, the precursor ion was observed at m/z 169.0149 $[M-H]^-$ (Figure 6A). The precursor ion underwent decarboxylation by losing CO_2 to generate the fragment ion at m/z 125.0266 $[M-H-CO_2]^-$. Subsequently, this fragment ion produced characteristic ions at m/z 107.0138 and m/z 97.0298 through the loss of H_2O and CO, respectively. Based on the accurate mass and fragmentation behavior reported in previous studies [50], compound **1** was tentatively identified as gallic acid ($C_7H_6O_5$).

Compound **2** showed a retention time of 4.20 min. In the negative ion mode, the precursor ion was detected at m/z 289.0718 $[M-H]^-$ (Figure 6B). The precursor ion initially underwent dehydration to produce the fragment ion at m/z 271.0614 $[M-H-H_2O]^-$. This ion further underwent fragmentation through the C-ring with the loss of CO_2, generating the ion at m/z 227.0713, or underwent C-ring heterocyclic ring fission to produce the characteristic fragment ion at m/z 203.0709. In addition, the precursor ion could directly lose CO_2 to form m/z 245.0806 $[M-H-CO_2]^-$, followed by C-ring RDA cleavage to generate the characteristic fragment ion at m/z 125.0245. The fragment ion at m/z 203.0709 further underwent B-ring cleavage to produce the low-mass diagnostic ion at m/z 109.0298, while m/z 227.0713 could undergo sequential neutral loss and skeletal rearrangement to generate m/z 205.0501. According to the fragmentation characteristics and literature data [51], compound **2** was tentatively identified as epicatechin.

Table 4. Preliminary identification of compounds in *Polygonum hydropiper* by UPLC-Q-TOF-MS/MS.

No.	t_R/min	Adduct	Name	Formula	Mass	Diagnostic Fragment Ions
1	1.43	−H	Gallic acid	$C_7H_6O_5$	170.0215	125.0266, 107.0138, 97.0298, 79.0199
2	4.20	−H	Epicatechin	$C_{15}H_{14}O_6$	290.0790	271.0614, 245.0806, 227.0713, 205.0501, 203.0709, 125.0245, 109.0298
3	5.10	−H	Hyperoside	$C_{21}H_{20}O_{12}$	464.0955	301.0406, 300.0391, 271.0290, 255.0319, 151.0047
4	5.10	+H	Quercetin	$C_{15}H_{10}O_7$	302.0427	285.0384, 257.0450, 229.0500, 165.0171, 153.0186
5	5.49	+H	Kaempferol	$C_{15}H_{10}O_6$	286.0477	258.0521, 165.0177, 153.0179, 121.0278
6	5.51	+H	Isorhamnetin	$C_{16}H_{12}O_7$	316.0583	302.0425, 285.0384, 257.0425, 229.0484, 153.0155
7	5.54	−H	kaempferol-3-*O*-Hexoside	$C_{21}H_{20}O_{11}$	448.1006	285.0421, 284.0351, 255.0321, 227.0365
8	6.87	+H	7,4′-Di-*O*-methylquercetin	$C_{17}H_{14}O_7$	330.0740	316.0577, 299.0542, 288.0621, 271.0596, 243.0650

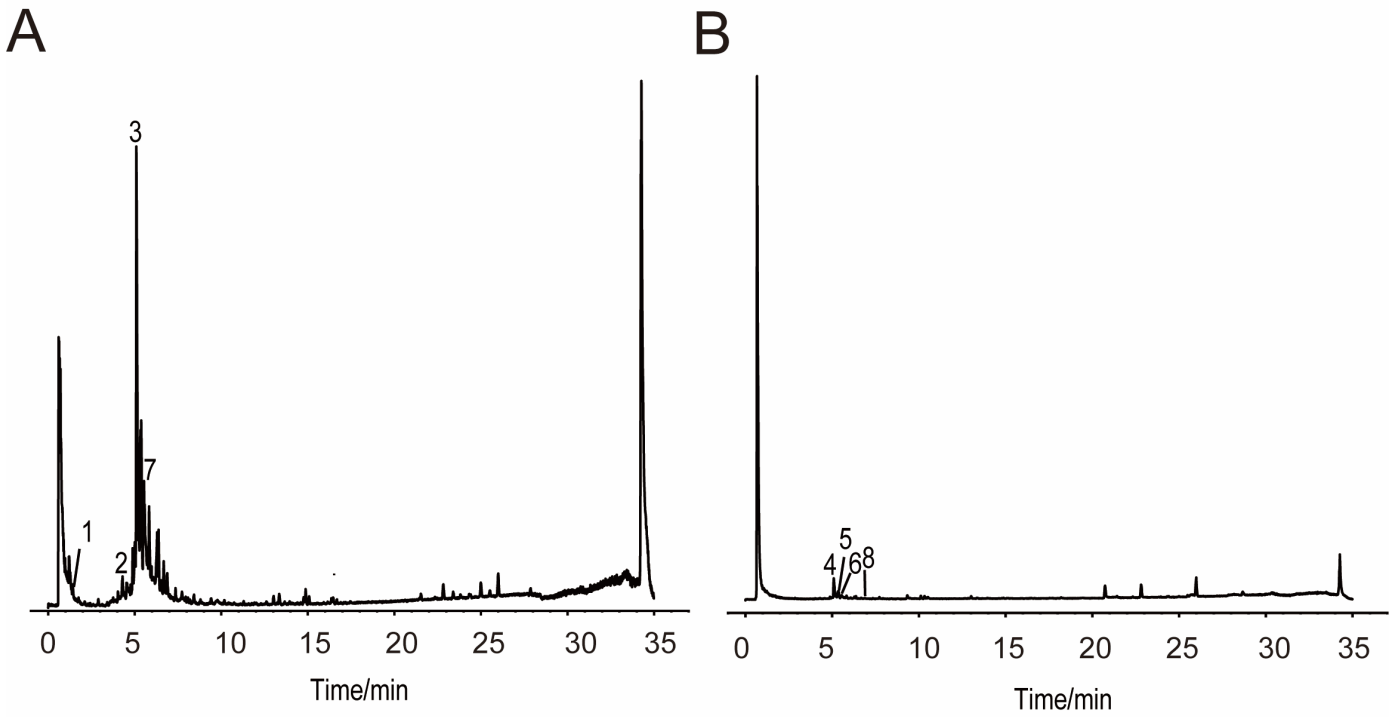


Figure 5. Total ion chromatogram (TIC) of flavonoids from *Polygonum hydropiper* determined by UPLC-Q-TOF-MS/MS. (**A**) Negative ion mode; (**B**) Positive ion mode. The numbered peaks (1–8) correspond to the compounds listed in Table 4.

Compound **3** was detected at a retention time of 5.10 min. In the negative ion mode, the precursor ion was observed at m/z 463.0878 $[M-H]^-$ (Figure 6C). The precursor ion underwent the loss of a hexose moiety ($C_6H_{10}O_5$) to generate the characteristic aglycone ion at m/z 301.0406 $[M-H-C_6H_{10}O_5]^-$, which further generated the characteristic fragment ion at m/z 151.0047 via RDA cleavage. On the other pathway, glycosidic bond homolytic cleavage yielded the characteristic radical aglycone ion at m/z 300.0391, a diagnostic ion for 3-*O*-glycosides. This radical aglycone ion at m/z 300.0391 underwent the loss of HCO to produce fragment ion at m/z 271.0290, or lost CO + OH to form fragment ion at m/z 255.0319. Based on the fragmentation pattern and reported literature [52], compound **3** was tentatively identified as hyperoside.

Compound **4** showed a retention time of 5.10 min. In the positive ion mode, the precursor ion was detected at m/z 303.0502 $[M^+H]^+$ (Figure 6D). The precursor ion underwent dehydration to form the fragment ion at m/z 285.0385 $[M^+H-H_2O]^+$, followed by succes-

sive losses of CO to generate fragment ions at m/z 257.0450 and m/z 229.0500. In addition, the precursor ion underwent RDA cleavage to produce characteristic fragment ions at m/z 165.0171 and m/z 153.0186. Based on the accurate mass and characteristic fragmentation pathways [53], compound **4** was tentatively identified as quercetin.

Compound **5** exhibited a retention time of 5.49 min. In the positive ion mode, the precursor ion was detected at m/z 287.0550 $[M^+H]^+$ (Figure 6E). The precursor ion underwent the loss of CHO to generate the fragment ion at m/z 258.0521 $[M^+H-CHO]^+$. Meanwhile, the precursor ion underwent RDA cleavage, producing characteristic fragment ions at m/z 153.0179 and m/z 121.0278. In addition, cleavage of the flavonoid skeleton through the loss of a neutral ring fragment generated the fragment ion at m/z 165.0177. Based on the accurate mass and characteristic fragmentation behavior reported in previous studies [54], compound **5** was tentatively identified as kaempferol.

Compound **6** was detected at a retention time of 5.51 min. In the positive ion mode, the precursor ion was observed at m/z 317.0655$[M^+H]^+$ (Figure 6F). The precursor ion underwent homolytic cleavage of the methyl radical ($CH_3\cdot$), producing the characteristic fragment ion at m/z 302.0425 $[M+H-CH_3]^{+\bullet}$. This fragment ion further underwent the loss of OH to generate the fragment ion at m/z 285.0384 $[M^+H-CH_3-OH]^+$. Subsequently, consecutive losses of two CO molecules produced fragment ions at m/z 257.0425 and m/z 229.0484. In addition, the precursor ion underwent RDA cleavage to generate the characteristic fragment ion at m/z 153.0155. According to the accurate mass and reported fragmentation characteristics [55], compound **6** was tentatively identified as isorhamnetin.

Compound **7** showed a retention time of 5.54 min. In the negative ion mode, the precursor ion was observed at m/z 447.0964 $[M-H]^-$ (Figure 6G). The precursor ion underwent the loss of a hexose moiety ($C_6H_{10}O_5$) to generate the aglycone ion at m/z 285.0421 $[M-H-C_6H_{10}O_5]^-$. Meanwhile, cleavage of the glycosidic bond through the loss of a hexose radical ($C_6H_{10}O_5\cdot$) generated the characteristic radical aglycone ion at m/z 284.0351 $[M-H-C_6H_{10}O_5]^{\cdot-}$. The radical aglycone ion further underwent the loss of CO and H· to produce the fragment ion at m/z 255.0321, followed by the loss of another CO molecule to generate the fragment ion at m/z 227.0365. Based on the accurate mass and characteristic fragmentation pathways [56], compound **7** was tentatively identified as kaempferol-3-*O*-hexoside.

Compound **8** exhibited a retention time of 6.87 min. In the positive ion mode, the precursor ion was detected at m/z 331.0818 $[M^+H]^+$ (Figure 6H). The precursor ion underwent the loss of a methyl radical ($CH_3\cdot$) to generate the characteristic fragment ion at m/z 316.0577 $[M+H-CH_3]^{+\bullet}$, which further lost one CO molecule to produce the fragment ion at m/z 288.0621. Meanwhile, the precursor ion could also undergo the loss of methanol (CH_3OH) to form the fragment ion at m/z 299.0542 $[M^+H-CH_3OH]^+$. This fragment ion subsequently underwent consecutive losses of two CO molecules, generating fragment ions at m/z 271.0596 and m/z 243.0650. Based on the accurate mass and reported fragmentation characteristics [57], compound **8** was tentatively identified as 7,4′-di-*O*-methylquercetin.

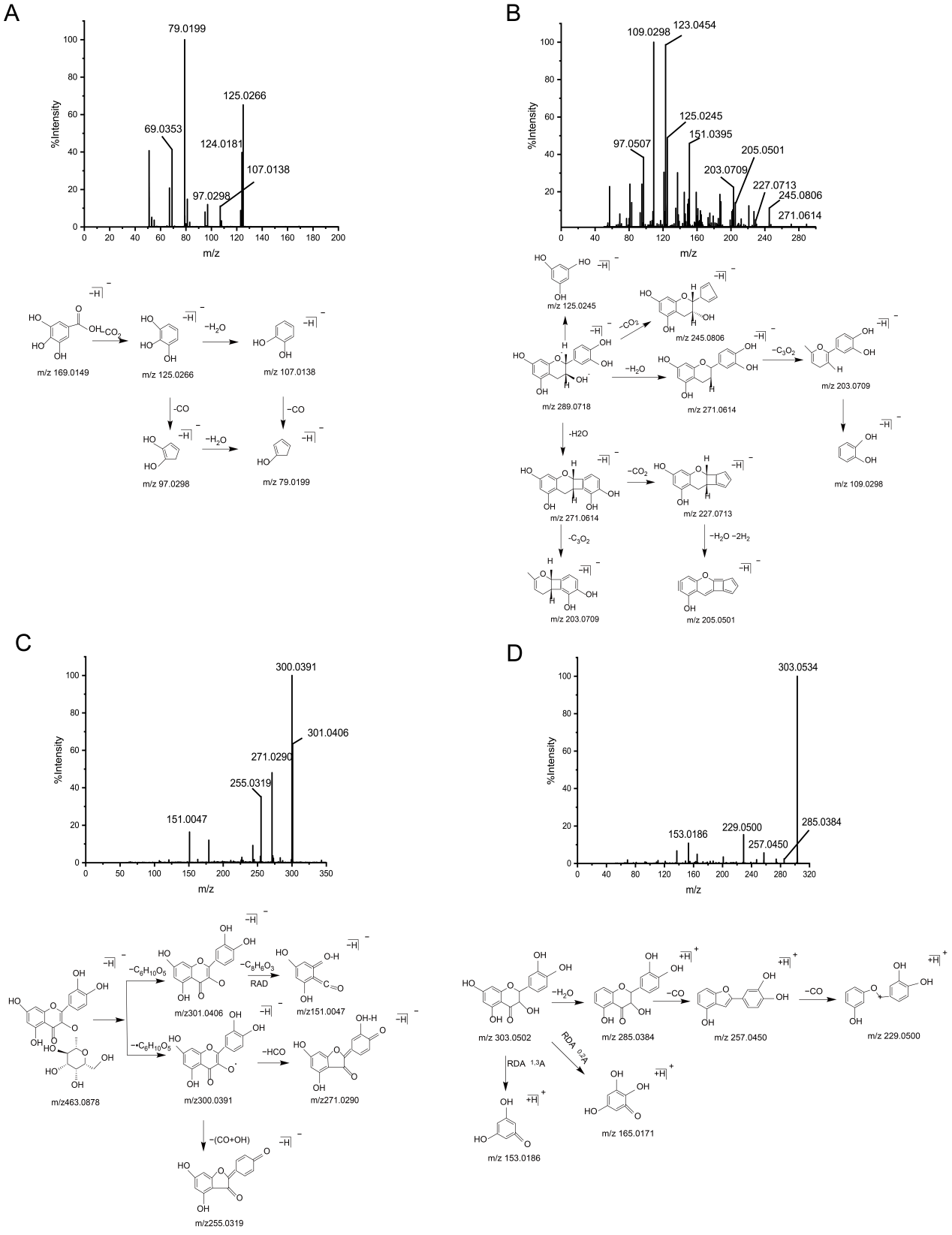


Figure 6. *Cont.*

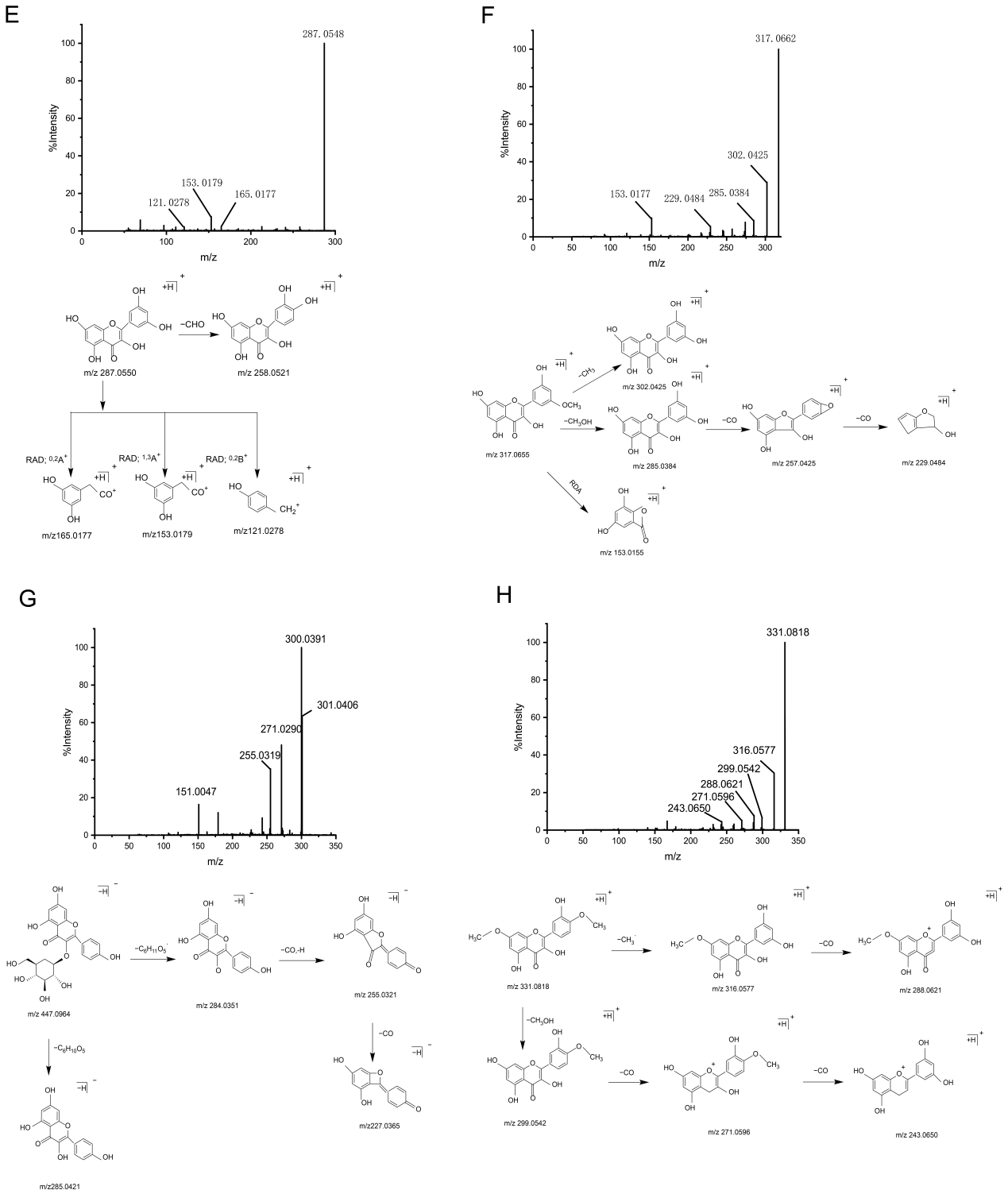


Figure 6. Proposed fragmentation pathways of the eight compounds identified in *Polygonum hydropiper* extracted with Bet-Gly. (**A**) Gallic acid; (**B**) Epicatechin; (**C**) Hyperoside; (**D**) Quercetin; (**E**) Kaempferol; (**F**) Isorhamnetin; (**G**) Kaempferol-3-*O*-hexoside; (**H**) 7,4′-Di-*O*-methylquercetin. The overlapping content in the figure (e.g., adjacent chemical structures) has been checked and does not affect the scientific understanding of the fragmentation pathways.

3.9. Molecular Dynamics Simulation Analysis

DESs are composed of hydrogen bond acceptors (HBAs) and hydrogen bond donors (HBDs) that can interact with polar functional groups, such as hydroxyl and carbonyl groups, in flavonoids through hydrogen bonding and other intermolecular

interactions, thereby improving the solvation of the target compounds. These interactions are regarded as important factors governing the extraction performance of DESs [58,59]. In this study, the extraction efficiency of total flavonoids followed the order Bet-Gly > 70% ethanol > water. To further elucidate the influence of different extraction media on flavonoid extraction at the molecular level, molecular dynamics (MD) simulations were performed. Water, Bet-Gly, and 70% ethanol were selected as representative solvent systems. Five major flavonoids identified in *P. hydropiper* (hyperoside, epicatechin, kaempferol, quercetin, and kaempferol-3-*O*-hexoside) were selected as model compounds, and 100 ns MD simulations were performed for each system. The dynamic behaviors and conformational snapshots at 0, 50, and 100 ns of the five flavonoids in the three solvent systems are shown in Figure 7A–C. The variation in the number of hydrogen bonds between individual flavonoids and each solvent system is shown in Figure 7d. Figure 7e shows the change in the total number of hydrogen bonds within each system. Figure 7D further compares the average interaction energies between the five flavonoids and the three solvent systems.

At 0 ns, all five flavonoid molecules were mainly distributed near the center of the simulation box in the three solvent systems. As the simulation proceeded, molecular rearrangement gradually occurred in all systems. At 50 ns, the flavonoids in the Bet-Gly system showed clear dispersion toward different regions. After 100 ns, marked local aggregation remained in the water system, whereas aggregation was reduced in the 70% ethanol system. In contrast, the five flavonoids exhibited the most uniform distribution in the Bet-Gly system, indicating that Bet-Gly was more favorable for maintaining the dispersed state of the flavonoid molecules. The hydrogen-bonding interactions between flavonoids and solvents were further analyzed (Figure 7d). Among the three solvent systems, hyperoside, kaempferol-3-*O*-hexoside, and epicatechin showed relatively higher numbers of hydrogen bonds, whereas quercetin and especially kaempferol formed fewer hydrogen bonds. These results suggest that the structural characteristics of different flavonoids play an important role in determining their hydrogen-bonding ability with the surrounding solvents. Similar observations were reported by Kohani et al. [18], who demonstrated that structural differences among bioactive compounds directly affected their ability to form hydrogen bonds with DES components. The higher numbers of hydrogen bonds observed for hyperoside and kaempferol-3-*O*-hexoside may be attributed to the presence of sugar moieties, whose multiple hydroxyl groups provide additional hydrogen bond donor and acceptor sites [60]. Epicatechin also contains several exposed hydroxyl groups, allowing it to form abundant hydrogen bonds with surrounding solvent molecules. In contrast, quercetin and kaempferol lack glycosyl groups and possess fewer oxygen-containing functional groups available for hydrogen bonding. Moreover, quercetin contains one additional hydroxyl group compared with kaempferol, which is consistent with its slightly higher number of hydrogen bonds in all three solvent systems. These results indicate that the hydrogen-bonding behavior of flavonoids is closely associated with the number of hydroxyl groups, the degree of glycosylation, and the accessibility of polar functional groups. Interestingly, the total number of hydrogen bonds in the water system was generally higher than in the Bet-Gly and 70% ethanol systems, indicating that the Water system possessed a stronger overall hydrogen-bond network (Figure 7e). However, the extraction yields obtained with water, 70% ethanol, and Bet-Gly were 1.72, 2.85, and 3.98 mg RE/g DW, respectively, suggesting that the number of hydrogen bonds formed between flavonoids and solvents alone cannot directly determine extraction efficiency. Xu et al. reported that flavonoid extraction efficiency was closely related to the solvent polarity and hydrogen bond donor properties of DESs, and that adjusting solvent polarity could improve the extraction of flavonoid glycosides and polymethoxylated flavonoids [20].

Therefore, solvent–solute polarity matching, rather than the number of hydrogen bonds alone, is an important factor influencing flavonoid extraction performance.

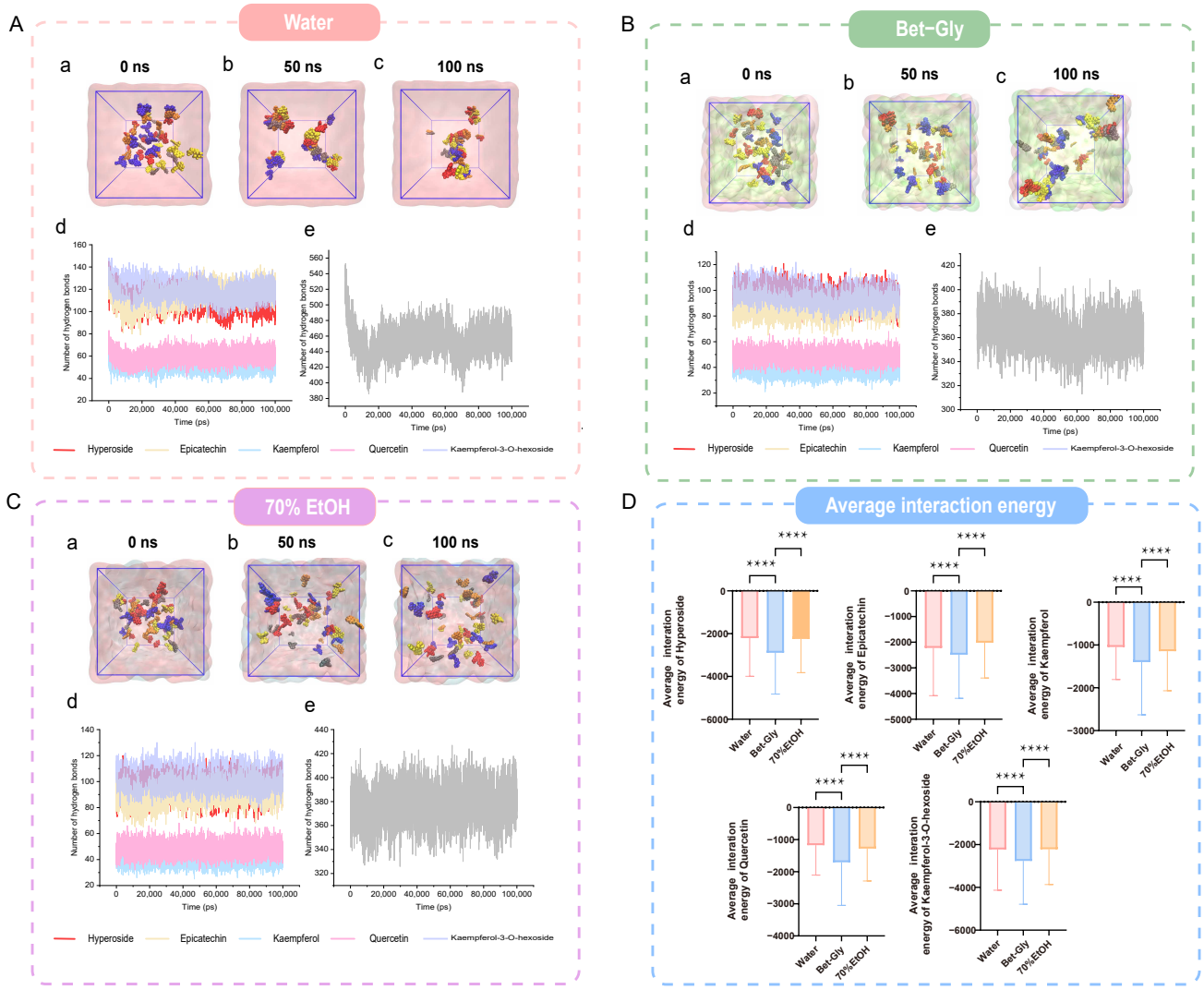


Figure 7. (**A**–**C**) represent the three solvent systems with internal subfigures (**a**–**e**), and (**D**) represents the average interaction energy. Molecular dynamics simulation analysis of the interactions between flavonoid constituents and different extraction solvents (water, Bet-Gly DES, and 70% ethanol). (**a**–**c**) Conformational snapshots at 0, 50, and 100 ns. (**d**) Number of hydrogen bonds between individual flavonoids and the solvent. (**e**) Average interaction energies between flavonoids and solvents. Different colors represent the three solvent systems. The asterisks (∗∗∗∗) indicate significant differences at $p < 0.0001$.

Based on these findings, the overall interaction energies between flavonoids and solvents were further compared to investigate whether Bet-Gly provided stronger molecular affinity (Figure 7D). The total interaction energy consists mainly of electrostatic and van der Waals interactions. Unlike the hydrogen-bond analysis, all five representative flavonoids exhibited significantly lower average total interaction energies in Bet-Gly than in Water and 70% ethanol ($p < 0.0001$). This trend was consistent for hyperoside, epicatechin, kaempferol, quercetin, and kaempferol-3-*O*-hexoside. The stronger interaction between flavonoids and Bet-Gly may be attributed to the unique multicomponent solvent environment of the DES. Betaine contains a zwitterionic structure with carboxylate and quaternary ammonium groups that provide strong electrostatic interaction sites, whereas glycerol

contains multiple hydroxyl groups that participate in dynamic hydrogen-bond networks. In addition, the presence of water in the DES system can reduce viscosity and facilitate molecular diffusion, allowing the HBA, HBD, and water molecules to collectively contribute to flavonoid solvation [40]. Fan et al. [61] reported that a betaine–glycerol system achieved higher extraction efficiency for chlorogenic acid from honeysuckle than ethanol extraction, and MD simulations demonstrated that extraction performance was closely associated with molecular interaction energy. Consistent with these findings, although the numbers of hydrogen bonds of flavonoids in Bet-Gly were not the highest among the three solvent systems, the combined contributions of electrostatic and van der Waals interactions resulted in more negative total interaction energies. Therefore, the betaine–glycerol-water DES microenvironment enhanced the overall solvation capability toward flavonoids through synergistic non-covalent interactions, making Bet-Gly a more suitable extraction medium for flavonoids from *P. hydropiper* than water and 70% ethanol.

4. Conclusions

The optimal extraction conditions were predicted to be a water content of 28.08%, a solid-to-liquid ratio of 1:37.58, and an extraction time of 30.69 min. For practical operation, these conditions were adjusted to a water content of 28.10%, a solid-to-liquid ratio of 1:38, and an extraction time of 31 min. Under the modified conditions, the experimental total flavonoid yield was 3.98 mg RE/g DW, in good agreement with the predicted value (4.13 mg RE/g DW). Compared with 70% ethanol and water, the optimized DES system significantly improved total flavonoid yield and exhibited stronger antioxidant activity. UPLC-Q-TOF-MS/MS tentatively identified eight compounds, mainly flavonoids, in the DES extract. Furthermore, molecular dynamics simulations revealed that the superior extraction performance of Bet-Gly was associated with more favorable flavonoid-solvent interactions, particularly electrostatic and van der Waals interactions. Overall, this study provides an integrated strategy combining DES extraction optimization, antioxidant evaluation, chemical profiling, and molecular simulation, offering a theoretical basis for the efficient utilization of flavonoids from *P. hydropiper*.

Author Contributions: Conceptualization, Y.S.; methodology, H.Z.; software, X.W.; validation, H.T. and H.Z.; formal analysis, H.T.; investigation, X.W.; resources, H.Z.; data curation, H.T.; writing—original draft preparation, X.W.; writing—review and editing, Y.S. and H.T.; visualization, X.W.; supervision, Y.S.; project administration, Y.S.; funding acquisition, Y.S. All authors have read and agreed to the published version of the manuscript.

Funding: This research was funded by the University-Level Scientific Research Funding Project of Hainan Vocational University of Science and Technology (No. HKKY2024-TD-10) and the 2025 College Students' Innovation Training Program of Hainan Vocational University of Science and Technology (Project: Study on the Mechanism of Action of Hainan Li Medicine Fengliao Changweikang in Treating Diarrhea). This work was also supported by the Li and Miao Medicine Research Platform and the University-Level Characteristic Key Discipline (Pharmacy) Construction Fund of Hainan Vocational University of Science and Technology.

Institutional Review Board Statement: Not applicable.

Informed Consent Statement: Not applicable.

Data Availability Statement: The data presented in this study are available upon request from the corresponding author.

Conflicts of Interest: The authors declare no conflicts of interest.

Abbreviations

The following abbreviations are used in this manuscript:

Bet-Gly	Betaine–glycerol
DES	Deep Eutectic Solvent
HBA	Hydrogen Bond Acceptor
HBD	Hydrogen Bond Donor
ABTS	2,2′-azino-bis (3-ethylbenzothiazoline-6-sulfonic acid)
DPPH	2,2-diphenyl-1-picrylhydrazyl
IC50	Half-maximal inhibitory concentration
UPLC-Q-TOF-MS/MS	Ultra-performance liquid chromatography-quadrupole time-of-flight tandem mass spectrometry
MD	Molecular dynamics
PHE-DES	*Polygonum hydropiper* extract-deep eutectic solvent
PHE-EtOH	*Polygonum hydropiper* extract-ethanol
PHE-Aq	*Polygonum hydropiper* extract-aqueous

Appendix A

Table A1. Plackett–Burman design matrix and experimental results for total flavonoid yield.

Std	Run	X1	X2	X3	X4	X5	Yield/(mg RE/g DW)
7	1	50	10	10	80	80	4.33
4	2	10	50	10	100	80	2.83
10	3	10	50	50	100	40	3.07
1	4	50	50	10	100	80	4.00
5	5	10	10	50	80	80	4.07
11	6	50	10	50	100	80	5.23
12	7	10	10	10	80	40	2.53
8	8	50	50	10	80	40	3.60
9	9	50	50	50	80	40	3.90
2	10	10	50	50	80	80	2.70
3	11	50	10	50	100	40	5.10
6	12	10	10	10	100	40	2.77

Table A2. Box–Behnken design matrix and experimental results for total flavonoid yield.

NO.	Water Content/%	Solid-to-Liquid Ratio	Extraction Time/min	Yield/(mg RE/g DW)
1	20	50	30	2.04
2	30	30	40	2.87
3	30	40	30	3.90
4	40	50	30	1.91
5	30	50	20	1.74
6	30	50	40	1.44
7	40	40	20	1.53
8	30	30	20	2.08
9	30	40	30	4.15
10	30	40	30	4.25
11	30	40	30	3.86
12	30	40	30	4.09
13	40	30	30	2.23
14	40	40	40	2.58
15	20	40	20	2.68
16	20	40	40	2.32
17	20	30	30	3.23

Table A3. IC_{50} values of antioxidant activity measured by ABTS and DPPH assays.

Sample	ABTS		DPPH	
	IC50 (mg/mL)	95% CI (mg/mL)	IC50 (mg/mL)	95% CI (mg/mL)
L-ascorbic acid	0.00970	0.00600∼0.0143	0.0414	0.0346∼0.0504
PHE-DES	0.4959	0.393∼0.708	3.5240	2.85∼4.38
PHE-EtOH	0.6660	0.590∼0.777	6.2250	4.64∼9.52
PHE-Aq	0.9031	0.796∼1.06	10.3200	8.73∼12.8

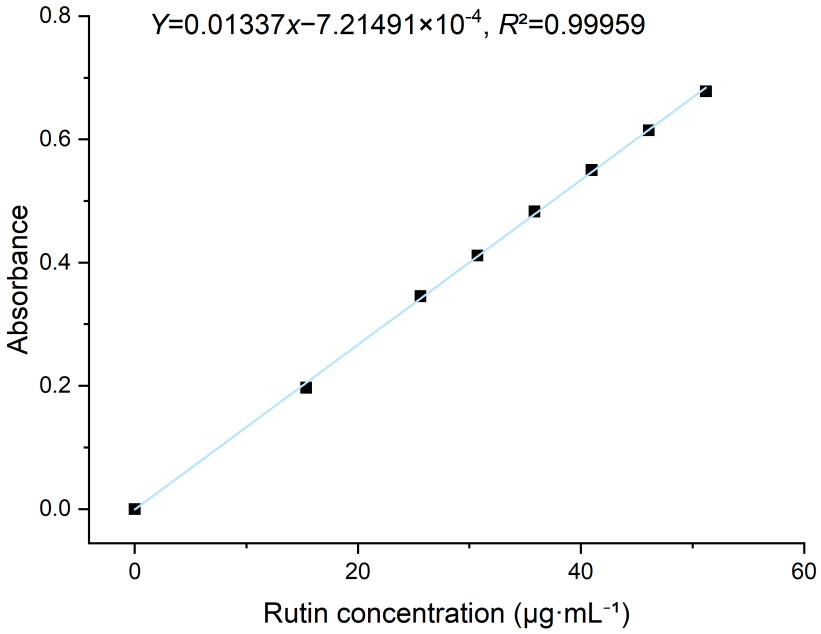


Figure A1. The calibration curve for rutin. The black squares represent the experimental data, and the light blue line represents the linear regression fit.

References

1. Kong, Y.D.; Qi, Y.; Cui, N.; Zhang, Z.H.; Wei, N.; Wang, C.F.; Zeng, Y.N.; Sun, Y.P.; Kuang, H.X.; Wang, Q.H. The Traditional Herb *Polygonum hydropiper* from China: A Comprehensive Review on Phytochemistry, Pharmacological Activities and Applications. *Pharm. Biol.* **2023**, *61*, 799–814. [CrossRef] [PubMed]
2. Shen, N.; Wang, T.; Gan, Q.; Liu, S.; Wang, L.; Jin, B. Plant Flavonoids: Classification, Distribution, Biosynthesis, and Antioxidant Activity. *Food Chem.* **2022**, *383*, 132531. [CrossRef] [PubMed]
3. Peng, Z. Antioxidant Flavonoids from Leaves of *Polygonum hydropiper* L. *Phytochemistry* **2003**, *62*, 219–228. [CrossRef] [PubMed]
4. Chemat, F.; Abert Vian, M.; Fabiano-Tixier, A.S.; Nutrizio, M.; Režek Jambrak, A.; Munekata, P.; Lorenzo, J.; Barba, F.; Binello, A.; Cravotto, G. A Review of Sustainable and Intensified Techniques for Extraction of Food and Natural Products. *Green Chem.* **2020**, *22*, 2325–2353. [CrossRef]
5. Abbott, A.; Capper, G.; Davies, D.; Rasheed, R.; Tambyrajah, V. Novel Solvent Properties of Choline Chloride/Urea Mixtures. *Chem. Commun.* **2003**, *39*, 70–71. [CrossRef] [PubMed]
6. Fernández, M.; Boiteux, J.; Espino, M.; Gomez, F.; Silva, M. Natural Deep Eutectic Solvents-Mediated Extractions: The Way Forward for Sustainable Analytical Developments. *Anal. Chim. Acta* **2018**, *1038*, 1–10. [CrossRef] [PubMed]
7. Choi, Y.; Van Spronsen, J.; Dai, Y.; Verberne, M.; Hollmann, F.; Arends, I.; Witkamp, G.J.; Verpoorte, R. Are Natural Deep Eutectic Solvents the Missing Link in Understanding Cellular Metabolism and Physiology? *Plant Physiol.* **2011**, *156*, 1701–1705. [CrossRef] [PubMed]
8. Dai, Y.; Van Spronsen, J.; Witkamp, G.J.; Verpoorte, R.; Choi, Y. Natural Deep Eutectic Solvents as New Potential Media for Green Technology. *Anal. Chim. Acta* **2013**, *766*, 61–68. [CrossRef] [PubMed]
9. Wen, C.; Zhang, J.; Zhang, H.; Dzah, C.; Zandile, M.; Duan, Y.; Ma, H.; Luo, X. Advances in Ultrasound Assisted Extraction of Bioactive Compounds from Cash Crops—A Review. *Ultrason. Sonochem.* **2018**, *48*, 538–549. [CrossRef] [PubMed]

10. Meng, Y.; Zou, W.; Guo, T.; Zhang, L.; Zhang, P.; Shu, P. Optimization of Ultrasound-Assisted Deep Eutectic Solvent Extraction, Characterization, and Bioactivities of Flavonoids from from *Cercis glabra* Leaves. *Ultrason. Sonochem.* **2025**, *120*, 107434. [CrossRef] [PubMed]
11. Wang, Z.; Wang, D.; Fang, J.; Song, Z.; Geng, J.; Zhao, J.; Fang, Y.; Wang, C.; Li, M. Green and Efficient Extraction of Flavonoids from *Perilla frutescens* (L.) Britt. Leaves Based on Natural Deep Eutectic Solvents: Process Optimization, Component Identification, and Biological Activity. *Food Chem.* **2024**, *452*, 139508. [CrossRef] [PubMed]
12. Wu, L.; Li, L.; Chen, S.; Wang, L.; Lin, X. Deep Eutectic Solvent-Based Ultrasonic-Assisted Extraction of Phenolic Compounds from *Moringa oleifera* L. Leaves: Optimization, Comparison and Antioxidant Activity. *Sep. Purif. Technol.* **2020**, *247*, 117014. [CrossRef]
13. Lv, J.; Zhou, W.; Sun, C.; Cao, Y.; Xia, Q.; Zhou, Z.; Liang, S.; Wang, M.; Qi, X. Ultrasound-Assisted Deep Eutectic Solvent Extraction of Flavonoids from Chinese Bayberry Leaves: Optimization, Molecular Mechanism, and Antioxidant Evaluation. *Food Chem.* **2026**, *512*, 148996. [CrossRef] [PubMed]
14. Mansur, A.; Song, N.E.; Jang, H.; Lim, T.G.; Yoo, M.; Nam, T. Optimizing the Ultrasound-Assisted Deep Eutectic Solvent Extraction of Flavonoids in Common Buckwheat Sprouts. *Food Chem.* **2019**, *293*, 438–445. [CrossRef] [PubMed]
15. Wang, Z.; Wang, S.; Chen, Y.; Liang, L.; Yang, L.; Zeng, L. Ultrasound-Assisted Betaine-Based Natural Deep Eutectic Solvents for Green Extraction of Total Phenols and Flavonoids from *Lithocarpus litseifolius*: Mechanistic Insights and Anti-Hyperuricemic Applications. *Food Res. Int.* **2025**, *220*, 117048. [CrossRef] [PubMed]
16. Kotha, R.; Tareq, F.; Yildiz, E.; Luthria, D. Oxidative Stress and Antioxidants—A Critical Review on In Vitro Antioxidant Assays. *Antioxidants* **2022**, *11*, 2388. [CrossRef]
17. Peng, W.; Wang, X.; Wang, W.; Wang, Y.; Huang, J.; Zhou, R.; Bo, R.; Liu, M.; Yin, S.; Li, J. Comparison, Optimization and Antioxidant Activity of Ultrasound-Assisted Natural Deep Eutectic Solvents Extraction and Traditional Method: A Greener Route for Extraction of Flavonoid from *Moringa oleifera* Lam. Leaves. *Ultrason. Sonochem.* **2024**, *109*, 107003. [CrossRef] [PubMed]
18. Kohani, M.; Raissi, H.; Zaboli, A.; Hashemzadeh, H. Exploring the Potential of Deep Eutectic Solvents for Extracting Bioactive Compounds from Tea: Insights from Molecular Dynamics Simulations. *J. Mol. Liq.* **2024**, *393*, 123589. [CrossRef]
19. Cheng, Y.; Zhao, H.; Cui, L.; Hussain, H.; Nadolnik, L.; Zhang, Z.; Zhao, Y.; Qin, X.; Li, J.; Park, J.; et al. Ultrasonic-Assisted Extraction of Flavonoids from Peanut Leave and Stem Using Deep Eutectic Solvents and Its Molecular Mechanism. *Food Chem.* **2024**, *434*, 137497. [CrossRef] [PubMed]
20. Xu, M.; Ran, L.; Chen, N.; Fan, X.; Ren, D.; Yi, L. Polarity-Dependent Extraction of Flavonoids from Citrus Peel Waste Using a Tailor-Made Deep Eutectic Solvent. *Food Chem.* **2019**, *297*, 124970. [CrossRef] [PubMed]
21. Wang, P.; Wang, K.; Li, T.; Zhang, S.; Wu, J.; Wu, F.; Fang, G.; Wu, C.; Liu, X. Ultrasonic-Assisted Deep Eutectic Solvents Extraction of Saponins from *Strobilanthes sarcorrhiza*: Process Optimization and Mechanistic Insights. *Chem. Eng. J.* **2026**, *529*, 173213. [CrossRef]
22. Wang, H.; Yang, D.; Zhao, L.; Bo, Y.; Guo, J.; Yang, X.; Sun, Y.; Gao, B.; An, M. Ultrasound-Assisted Deep Eutectic Solvent Extraction of Flavonoids from *Spatholobi Caulis*: Optimization and Functional Assessment. *Microchem. J.* **2026**, *221*, 117042. [CrossRef]
23. Gomez, A.V.; Biswas, A.; Tadini, C.C.; Furtado, R.F.; Alves, C.R.; Cheng, H.N. Use of Natural Deep Eutectic Solvents for Polymerization and Polymer Reactions. *J. Braz. Chem. Soc.* **2019**, *30*, 717–726. [CrossRef]
24. Peng, Z.; Wang, Y.; Li, W.; Zhan, B.; Zhu, L.; Yang, D.; Li, G.; Zhang, L.; Zhao, Z. Ultrasonic-assisted extraction of flavonoids from *Amomum villosum* Lour. Using natural deep eutectic solvent: Process optimization, comparison, identification, and bioactivity. *Ultrason. Sonochem.* **2025**, *116*, 107304. [CrossRef] [PubMed]
25. Zuo, Y.F.; Wang, C.; Zhang, Q.; Wang, M.H.; Shan, T.Y.; Wang, C.C.; Li, J. Deep eutectic solvent-based ultrasonic-assisted extraction of three antioxidant flavonoids from *Sophorae Fructus*. *Chin. J. Anal. Chem.* **2026**, *54*, 100659. [CrossRef]
26. Yang, W.; Jiang, S.; Wu, X.; He, Y.; Peng, C.; Zhu, C.; Du, R.; Yuan, H.; Lan, S.; Liu, Z.; et al. Ultrasound-Assisted Deep Eutectic Solvent Extraction of Ginseng Folium Polysaccharides: Extraction Mechanism, Process Optimization, Structural Characterization, and In Vitro Biological Activity. *Ultrason. Sonochem.* **2026**, *127*, 107797. [CrossRef] [PubMed]
27. Guo, X.D.; Ma, Y.J.; Parry, J.; Gao, J.M.; Yu, L.L.; Wang, M. Phenolics Content and Antioxidant Activity of Tartary Buckwheat from Different Locations. *Molecules* **2011**, *16*, 9850–9867. [CrossRef] [PubMed]
28. Christodoulou, M.; Orellana Palacios, J.; Hesami, G.; Jafarzadeh, S.; Lorenzo, J.; Domínguez, R.; Moreno, A.; Hadidi, M. Spectrophotometric Methods for Measurement of Antioxidant Activity in Food and Pharmaceuticals. *Antioxidants* **2022**, *11*, 2213. [CrossRef] [PubMed]
29. Tian, L. Sobtop. Available online: http://sobereva.com/soft/Sobtop (accessed on 22 October 2025).
30. Neese, F. Software Update: The ORCA Program System, Version 4.0. *WIREs Comput. Mol. Sci.* **2018**, *8*, e1327. [CrossRef]
31. Lu, T.; Chen, F. Multiwfn: A Multifunctional Wavefunction Analyzer. *J. Comput. Chem.* **2012**, *33*, 580–592. [CrossRef] [PubMed]
32. Martínez, L.; Andrade, R.; Birgin, E.; Martínez, J. PACKMOL: A Package for Building Initial Configurations for Molecular Dynamics Simulations. *J. Comput. Chem.* **2009**, *30*, 2157–2164. [CrossRef] [PubMed]

33. Hess, B. P-LINCS: A Parallel Linear Constraint Solver for Molecular Simulation. *J. Chem. Theory Comput.* **2008**, *4*, 116–122. [CrossRef] [PubMed]
34. Darden, T.; York, D.; Pedersen, L. Particle Mesh Ewald: An N log(N) Method for Ewald Sums in Large Systems. *J. Chem. Phys.* **1993**, *98*, 10089–10092. [CrossRef]
35. Parrinello, M.; Rahman, A. Polymorphic Transitions in Single Crystals: A New Molecular Dynamics Method. *J. Appl. Phys.* **1981**, *52*, 7182–7190. [CrossRef]
36. Miyamoto, S.; Kollman, P. Settle: An Analytical Version of the SHAKE and RATTLE Algorithm for Rigid Water Models. *J. Comput. Chem.* **1992**, *13*, 952–962. [CrossRef]
37. Humphrey, W.; Dalke, A.; Schulten, K. VMD: Visual Molecular Dynamics. *J. Mol. Graph.* **1996**, *14*, 33–38. [CrossRef] [PubMed]
38. Schrödinger, LLC. *The PyMOL Molecular Graphics System*, Version 3.0; Schrödinger, LLC.: New York, NY, USA, 2023.
39. Tang, W.; Wu, Y.; Wang, M.; Row, K.; Qiu, H.; Zhou, J.L. Emerging Application of Extraction Phase of Ionic and Non-Ionic Deep Eutectic Solvents toward Natural Herbal Medicine. *TrAC Trends Anal. Chem.* **2023**, *165*, 117137. [CrossRef]
40. Monteiro, H.; Paiva, A.; Duarte, A.; Galamba, N. Structure and Dynamic Properties of a Glycerol–Betaine Deep Eutectic Solvent: When Does a DES Become an Aqueous Solution? *ACS Sustain. Chem. Eng.* **2022**, *10*, 3501–3512. [CrossRef] [PubMed]
41. Hammond, O.; Bowron, D.; Edler, K. The Effect of Water upon Deep Eutectic Solvent Nanostructure: An Unusual Transition from Ionic Mixture to Aqueous Solution. *Angew. Chem. Int. Ed.* **2017**, *56*, 9782–9785. [CrossRef] [PubMed]
42. Kumar, K.; Srivastav, S.; Sharanagat, V. Ultrasound Assisted Extraction (UAE) of Bioactive Compounds from Fruit and Vegetable Processing by-Products: A Review. *Ultrason. Sonochem.* **2021**, *70*, 105325. [CrossRef] [PubMed]
43. Dzah, C.; Duan, Y.; Zhang, H.; Wen, C.; Zhang, J.; Chen, G.; Ma, H. The Effects of Ultrasound Assisted Extraction on Yield, Antioxidant, Anticancer and Antimicrobial Activity of Polyphenol Extracts: A Review. *Food Biosci.* **2020**, *35*, 100547. [CrossRef]
44. Fokuhl, V.; Kahl, L.; Heise, N.; Glomb, M. Singlet Oxygen Generated by Quercetin and Gallic Acid Leads to Oxidative Fragmentation of Flavonols in Onions and Leek. *J. Agric. Food Chem.* **2026**, *74*, 5640–5650. [CrossRef] [PubMed]
45. Shen, L.; Pang, S.; Zhong, M.; Sun, Y.; Qayum, A.; Liu, Y.; Rashid, A.; Xu, B.; Liang, Q.; Ma, H.; et al. A Comprehensive Review of Ultrasonic Assisted Extraction (UAE) for Bioactive Components: Principles, Advantages, Equipment, and Combined Technologies. *Ultrason. Sonochem.* **2023**, *101*, 106646. [CrossRef] [PubMed]
46. Mohd Fuad, F.; Mohd Nadzir, M.; Harun@Kamaruddin, A. Hydrophilic Natural Deep Eutectic Solvent: A Review on Physico-chemical Properties and Extractability of Bioactive Compounds. *J. Mol. Liq.* **2021**, *339*, 116923. [CrossRef]
47. Wei, J.; Zhao, G.; Wu, G.; Bo, Y.; Yang, D.; Guo, J.; Ma, Y.; An, M. An Ultrasound-Assisted Extraction Using an Alcohol-Based Hydrophilic Natural Deep Eutectic Solvent for the Determination of Five Flavonoids from *Platycladi Cacumen*. *Microchem. J.* **2024**, *198*, 110076. [CrossRef]
48. Xiong, Q.; Guo, D.; Song, E.; Yu, S.; Wang, M.; Fan, K.; Zhang, Z.; Zhang, X. Ultrasound-Assisted and Natural Deep Eutectic Solvent-Based Green Extraction of Total Flavonoids from *Artemisia argyi* with Enhanced Antioxidant Activity. *Microchem. J.* **2026**, *228*, 118989. [CrossRef]
49. Dai, H.; Hu, M.; Zhu, N.; Song, L.; Hong, H. Extraction of Flavonoids from *Artemisia argyi* Using Deep Eutectic Solvents and Its Antioxidant Activities. *J. Mol. Liq.* **2025**, *426*, 127236. [CrossRef]
50. Wang, S.; Sun, X.; An, S.; Sang, F.; Zhao, Y.; Yu, Z. High-Throughput Identification of Organic Compounds from Polygoni Multiflori Radix Praeparata (*Zhiheshouwu*) by UHPLC-Q-Exactive Orbitrap-MS. *Molecules* **2021**, *26*, 3977. [CrossRef] [PubMed]
51. Xu, F.; Liu, Y.; Song, R.; Dong, H.; Zhang, Z. Constituents of Da-Cheng-Qi Decoction and Its Parent Herbal Medicines Determined by LC-MS/MS. *Nat. Prod. Commun.* **2010**, *5*, 1934578X1000500522. [CrossRef]
52. Ji, L.; Shi, W.; Li, Y.; He, J.; Xu, G.; Qin, M.; Guo, Y.; Ma, Q. Systematic Identification, Fragmentation Pattern, and Metabolic Pathways of Hyperoside in Rat Plasma, Urine, and Feces by UPLC-Q-Exactive Orbitrap MS. *J. Anal. Methods Chem.* **2022**, *2022*, 2623018. [CrossRef] [PubMed]
53. Scigelova, M.; Hornshaw, M.; Giannakopulos, A.; Makarov, A. Fourier Transform Mass Spectrometry. *Mol. Cell. Proteom.* **2011**, *10*, M111.009431. [CrossRef] [PubMed]
54. Le, K.; Chiu, F.; Ng, K. Identification and Quantification of Antioxidants in *Fructus lycii*. *Food Chem.* **2007**, *105*, 353–363. [CrossRef]
55. Wei, L.; Ma, R.; Fu, Y. Differences in Chemical Constituents between *Dalbergia oliveri* Heartwood and Sapwood and Their Effect on Wood Color. *Molecules* **2022**, *27*, 7978. [CrossRef] [PubMed]
56. Dantas, C.; Abreu, L.; Da Cunha, H.; Veloso, C.; Souto, A.; De Fátima Agra, M.; De Oliveira Costa, V.; Da Silva, M.; Tavares, J. Dereplication of Phenolic Derivatives of Three *Erythroxylum* Species Using Liquid Chromatography Coupled with ESI-MSn and HRESIMS. *Phytochem. Anal.* **2021**, *32*, 1011–1026. [CrossRef] [PubMed]
57. Zhao, Q.; Li, Y.; Li, S.; He, X.; Gu, R. Comparative Bioactivity Evaluation and Metabolic Profiling of Different Parts of *Duhaldea nervosa* Based on GC-MS and LC-MS. *Front. Nutr.* **2023**, *10*, 1301715. [CrossRef] [PubMed]
58. Vora, Y.; Prajapati, M.; Bhavya, K.; Pal, D.; Kumar, K.; Kuperkar, K. Deep Eutectic Solvent-Mediated Solubilization Enhancement of Quercetin: Experimental, Molecular Dynamics, and Biological Evaluation. *J. Mol. Liq.* **2026**, *448*, 129384. [CrossRef]

59. Geara, D.; Fayad, S.; Chebil, L.; Harb, W. Molecular Interactions of Quercetin in Menthol-Based Type V Deep Eutectic Solvents: An Integrated FTIR Spectroscopy and Molecular Dynamics Study. *J. Mol. Liq.* **2026**, *457*, 129714. [CrossRef]
60. Lai, X.; Li, X.; Chen, J.; Liu, X.; Pan, P.; Zhou, Y.; Zhao, G. Advances in Flavonoid Glycosylation: Chemical and Biological Basis, Mechanisms, Physicochemical Properties, and Applications in the Food Industry. *Trends Food Sci. Technol.* **2025**, *165*, 105296. [CrossRef]
61. Fan, Z.; Li, J.; Zhou, J.; Chen, Y.; Cui, Z. Extraction of Chlorogenic Acid from *Lonicera japonica* Thunb. Thunb. Using Deep Eutectic Solvents: Process Optimization and Mechanism Exploration by the Combination of Experiment and Molecular Simulation. *Microchem. J.* **2025**, *212*, 113280. [CrossRef]

Disclaimer/Publisher's Note: The statements, opinions and data contained in all publications are solely those of the individual author(s) and contributor(s) and not of MDPI and/or the editor(s). MDPI and/or the editor(s) disclaim responsibility for any injury to people or property resulting from any ideas, methods, instructions or products referred to in the content.